High-power impulse magnetron re-sputtering/sputtering apparatus for Nb-Cu 1.3 GHz RF cavities

Peng Dong[1,2#], Yanjiang Wang[1,2#], Jianjun Xiao[1,2#], Meiling Bao[3#], Xin Liu[3], Zhaoxi Chen[2,4,a)], Jinfang Chen[4], Dong Wang[4], Xuerong Liu[4, a)], Yulin Chen[1,2], Zhi Liu[2,4], Jun Li[1,2,a)]

[1]ShanghaiTech Laboratory for Topological Physics, School of Physical Science and Technology, ShanghaiTech University, Shanghai 201210, China
[2] State Key Laboratory of Quantum Functional Materials, School of Physical Science and Technology, ShanghaiTech University, Shanghai 201210, China
[3] Zhuoling Precision Equipment (Hefei) Co. Ltd., Hefei, 230093, China
[4] Center for Transformative Science (CTS), Shanghai 201210, China

ABSTRACT

Superconducting radio frequency (SRF) cavities constitute the cornerstone of high-efficiency particle accelerators. While traditional bulk niobium cavities have dominated the field, copper substrates with niobium films deposited inside the cavity represent a transformative approach for cost reduction and thermal management. However, achieving conformal superconducting films on complex cavity geometries remains a fundamental challenge, especially on the adhesive behavior of the film. Here, we present a breakthrough high-power impulse magnetron re-sputtering/sputtering (HiPIMRS) system engineered for uniform Nb films deposition on 1.3 GHz copper cavity interiors. Through a re-sputtering process on the copper substrates prior to deposition, we achieve atomic-scale interfacial integrity, and eliminate interfacial oxides or degradation. Energy-dispersive X-ray spectroscopy confirms an oxide-free Nb/Cu interface, and atomic force microscopy reveals ultra-smooth surfaces (R_a < 20 nm for 3 μm films). Crucially, electrical transport measurements show that the niobium film has a critical temperature of 8.5 K throughout the cavity interior. XRD demonstrates a (110)-oriented crystalline structure. This work establishes HiPIMRS as a viable pathway for next-generation SRF cavity production, with interfacial engineering protocols offering generational advancements in film conformity and superconducting performance.

[a)] Author to whom correspondence should be addressed: chenzhx@shanghaitech.edu.cn; liuxr@shanghaitech.edu.cn; lijun3@shanghaitech.edu.cn

I. INTRODUTION

Superconducting radio frequency (SRF) cavities are indispensable components in quantum computing infrastructures, modern particle accelerators, and other emerging applications necessitating efficient particle acceleration [1-4]. Characterized by their high efficiency, high acceleration gradient, and extended operational lifetime, these cavities have emerged as crucial tools across a broad spectrum of scientific and technological domains[3, 5]. Bulk niobium (Nb) has been the material of choice for SRF cavity applications, primarily due to its high critical temperature (9.25 K), low surface resistance (R_s) and facile fabrication process. Decades of development have brought SRF cavity performance close to the theoretical limit of bulk niobium[6]. Consequently, there has been a resurgence of interest in thin-film alternatives and methodologies as substitutes for bulk niobium in the manufacture of superconducting radio frequency (SRF) cavities[7-9].

Copper-based niobium films cavities provide significant advantages over bulk niobium cavities, including reduced material costs, enhanced thermal conductivity for efficient heat dissipation, superior mechanical properties, and precise control of layer thickness through films deposition techniques[10] [11-13]. Depositing high-quality Nb films on Cu cavities necessitates uniform coverage in high-aspect-ratio structures and strong adhesion to Cu substrates. Up to now, several advanced deposition techniques have been developed for Nb film grown inside Cu cavities, including the vacuum arc deposition, electron cyclotron resonance (ECR) plasma, and high power impulse magnetron sputtering (HiPIMS) [14] [15-17]. Among these techniques, the HiPIMS, pioneered by CERN [11, 18], has spurred subsequent research efforts. These include the optimization of 1.3 GHz cavities using HiPIMS [14], achieving accelerating gradients up to 21 MV/m, and a critical milestone of 1.3 GHz Nb-Cu cavities with quality factors $Qo > 1\times10^{10}$ at 2.0 K [17]. However, Nb films often exhibit significant residual resistance (R_{res}) and a Q-slope [19, 20], limiting their performance at higher fields. The microscopic origin of the Q-slope phenomenon is multifactorial. However, preventing Cu substrate oxidation and interface degradation is universally acknowledged as a pivotal strategy for enhancing performance [21-25]. Previous studies demonstrated that Cu cavities have been polished by both mechanical and polyethylene wax techniques, however, the polished Cu cavities will be exposure in atmosphere and an oxidation layer will always exist at the surface, resulting in unavoidable problem of interfacial degradation. To eliminate this problem, an in-situ surface cleaning technique is essential to be developed [26, 27].

In this work, we present a novel high-power impulse magnetron re-sputtering/sputtering (HiPIMRS) facility engineered for the fabrication of 1.3 GHz Nb-Cu SRF cavities. The system integrates a tunable magnetron with translational target positioning, dynamic power control, and optimized magnetic field configurations to enable conformal niobium film deposition on complex copper cavity geometries under ultra-high vacuum conditions ($<10^{-7}$ Pa). Crucially, the apparatus incorporates in situ substrate re-sputtering capabilities for oxide layer free and atomic-scale interfacial preparation. The superconducting Nb films are observed with a high critical temperature of 8.5 K, flat surface roughness (R_a) < 12 nm (for 3 μm films),

and preferred crystallographic orientation along (110). This work demonstrates unprecedented control over film uniformity and interface integrity, establishing HiPIMRS as a scalable pathway for next-generation SRF cavities via direct energetic condensation.

II. SYSTEM DESIGN

A. Instrument overview

Figure 1a shows the structural configuration of the HiPIMRS apparatus engineered for conformal Nb thin-film deposition on 1.3 GHz Cu radio frequency (SRF) cavities. The system integrates a water-cooled magnetron target assembly within a 316 stainless steel ultra-high vacuum (UHV) chamber. A high-precision linear translation stage (resolution: ±0.1 mm) positions the target axially via vacuum feedthroughs, enabling localized sputtering within the SRF cavity geometry. All demountable flanges employ metal-sealed ConFlat® fittings (e.g., Cu gaskets) to maintain UHV integrity ($<10^{-7}$ Pa base pressure). The copper SRF cavity substrate is electrically isolated by alumina ceramic insulators and centrally suspended within the chamber. Vacuum generation combines a turbomolecular pump (500 L/s) for rapid pump-down and an ion pump (200 L/s) for stable UHV operation, isolated by a gate valve during high-pressure processes. The 3D schematics of the corresponding instrumentation are delineated in Figure 1b. The coating chamber features multiple preconfigured ports, which allow for the integration of supplementary instrumentation such as vacuum diagnostic modules, residual gas analyzers, and auxiliary electrodes.

The stainless-steel vacuum chamber features pre-installed flange ports for future expansions. It is equipped with high-power ion pumps and two sets of 1000 Hz turbo molecular pumps at its bottom and sides to ensure the cavity's vacuum requirements. After a two-day bakeout and cooling, the chamber achieves vacuum levels below 10^{-8} pascal, offering an ultra-high-vacuum (UHV) condition for controlled film deposition.

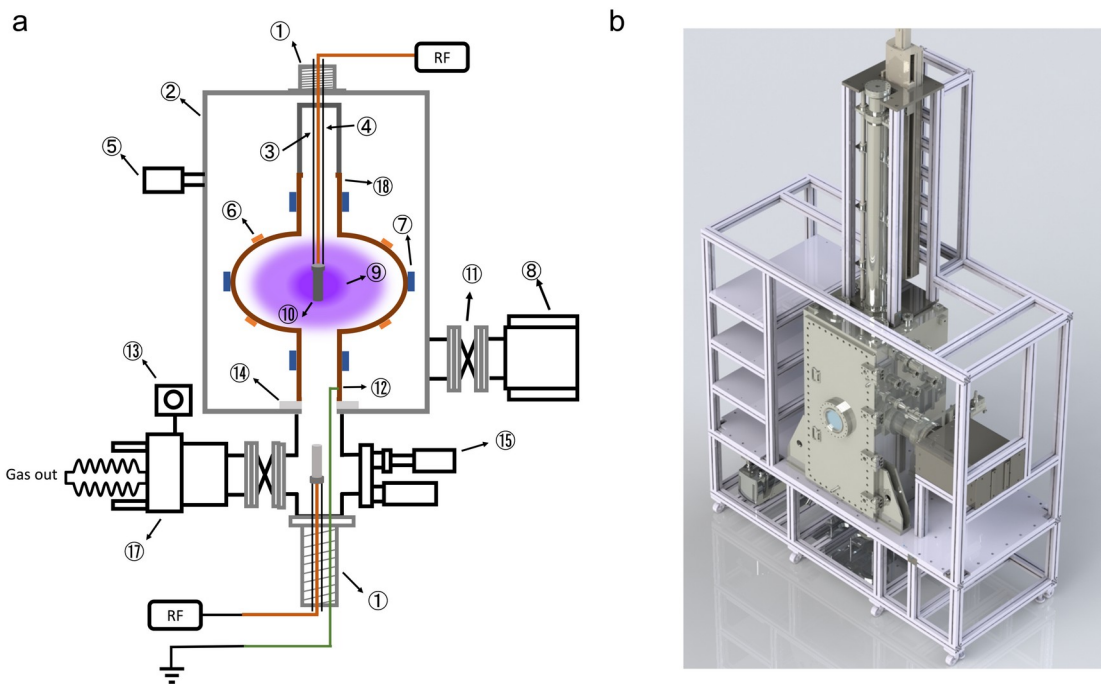

Figure 1. Schematic diagrams of the modular high-energy pulsed magnetron re-sputtering/sputtering (HiPIMRS) apparatus. (a) The integrated chamber design enabling substrate heating, re-sputtering cleaning, and film deposition. The labeled components and function within the vacuum chamber are as follows: 1. Translation stage; 2. Vacuum chamber; 3. Gas circuit; 4. Water circuit; 5. Vacuum gauge; 6. Temperature sensor; 7. Tantalum heater; 8. Ion pump; 9. Plasma; 10. Target; 11. Gate value; 12. Anode; 13. Mechanical pump; 14. Ceramic; 15. Residual Gas Analyzer; 16. Forevacuum gauge; 17. Molecular pump; 18. Cavity; (b) An outer-view of the designed apparatus.

B. Magnetron Sputtering Target System

The complex geometry of the 1.3 GHz SRF cavity leads to variations in target-substrate distances during sputtering, posing a persistent challenge for the uniform and adhesion of superconducting films on cavity internal surfaces. To address this challenge, an adaptable magnetron sputtering target system was developed. Figure 2a illustrates the functional design of the movable target insert, comprising an integrated niobium target, electrical circuits, gas supply lines, and cooling water channels essential for energetic condensation. The specific details are as follows:

(1) The uppermost four-way connector interfaces with an external power supply, process gas, and water chiller, sealed by a vacuum gasket. The high-precision positioning stage enables precise positional control of the target system with an accuracy of 0.1 millimeters (Figure 2a). The upper connecting rod, linked to the displacement stage, facilitates vertical movement of the magnetron target over a range of 1.0 meter, enabling full coverage of re-sputtering treatment and film deposition within the 1.3 GHz single-cell SRF cavity (length ~ 50 cm).

(2) The integrated niobium target consists of a high-purity niobium cylindrical tube (RRR > 300) serving as the cathode (Figure 2b). Inside, ring-shaped neodymium-iron-boron (NdFeB) magnets are isolated by ceramic spacers. The

magnets configuration is designed to enhance magnetic field distribution and sputtering performance by preventing dissipation at the magnet interfaces and dispersing normal field lines to the niobium cylindrical tube surface for enhanced secondary electrons. At the bottom, a ceramic substrate and central cooling device support the niobium tube, while a ceramic insulator at the top separates the gas inlet plate from the niobium target to prevent short-circuiting.

(3) Supplementary wires and channels are integrated to the target via cylindrical connectors as illustrated in Figure 2b. A water-cooling device in the center of the niobium cylinder transfers heat away from ion bombardment, preventing magnet demagnetization. The gas inlet plate, perforated around its perimeter, ensures uniform gas distribution and sputtering using high-precision flow meters to control the gas intake rate.

(4) The target system is equipped with a complementary sputtering power supply unit, which offers high and widely adjustable power. It supports a wide range of duty cycles and pulse frequencies, as well as the capability to modulate multiple pulse waveforms, including both positive and negative waveforms [28].

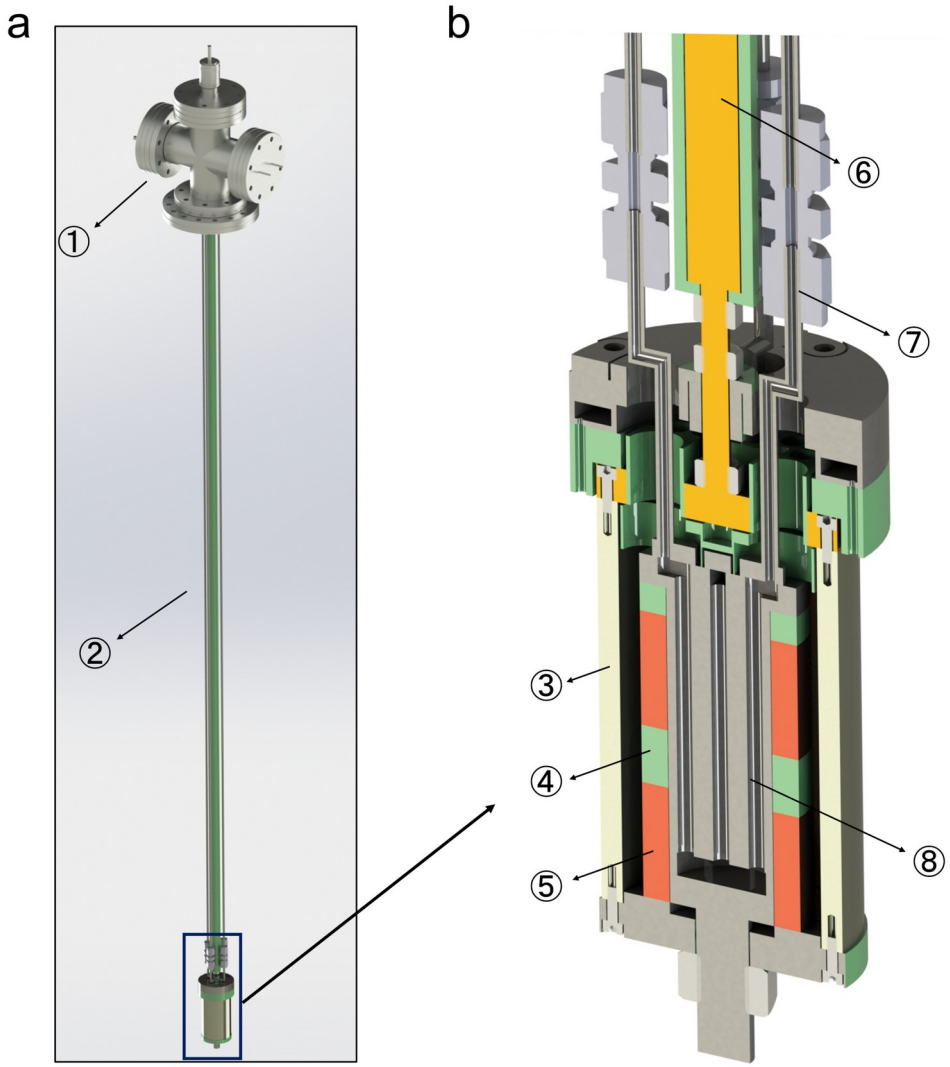

Figure 2. The sputtering module for HiPIMRS apparatus. (a) Configuration of the magnetron sputtering insert comprising a displacement linkage and a cathode (target). Element ① denotes the four-way connector, which is connected with an external power supply, process gas, and water chiller and enables control over the positioning of the target (b) with the high-precision positioning stage within the vacuum chamber. Element ② represents power supply, process gas, and water chiller. (b) The target connector of the magnetron sputtering apparatus, comprising element ③: the niobium target material; element ④: insulating ceramic tile; ⑤: the NdFeB magnet; ⑥: the copper electrode; ⑦: the cooling water channels; ⑧: Stainless Steel Coolant Reservoir. These components collectively facilitate the glow discharge process of the target during sputtering.

C. Multi-step sputtering process for the HiPIMRS technique

In the Nb-Cu SRF cavities, the Nb/Cu interface critically governs both superconducting performance and film adhesion. Conventional chemical and electrochemical polishing methods inherently permit native oxide formation (Cu_2O/CuO) during atmospheric transfer, introducing interfacial impurities that degrade film coherence and increase flux penetration[28, 29]. These oxides act as

flux-pinning centers and thermal barriers, elevating residual resistance and limiting achievable accelerating gradients [30]. To overcome this limitation, we developed an *in-situ* re-sputtering technique using a dual-target (Nb/Ti) magnetron system. As illustrated in Figure 3, this process enables:

Step 1, Ti-target pre-sputtering. Prior to niobium deposition, a titanium target was positioned at the base of the SRF cavity (Figure 3a) for *in-situ* vacuum enhancement. During a 2-minute pre-sputtering phase, freshly deposited titanium films functioned as active getters, chemically binding residual gases (primarily O_2, H_2O, CO). This reduced the operational pressure from an initial base pressure of 10^{-6} Pa to $\leq 10^{-7}$ Pa. This gettering mechanism suppressed interfacial oxygen contamination critical for Nb/Cu adhesion and superconducting performance.

Step 2, Ti-target re-sputtering. During the in-situ re-sputtering phase (Figure 3b), the Ti-target is positioned at the cavity center and electrically grounded, serving as the anode. The copper cavity functions as the RF-powered cathode (40 kHz), establishing an asymmetric electric field that ignites an argon plasma at 0.5 Pa. Positively charged argon ions (Ar^+) are accelerated across the cathode sheath, gaining ~50–200 eV kinetic energy before bombarding the copper surface. This controlled ion etching effectively removes particulate contaminants and native oxides (Cu_2O/CuO) while minimizing substrate heating. Crucially, the combination of low discharge power (60 W DC equivalent) and elevated pressure (0.5 Pa) prevented the deposition of impurities from copper surface sputtering onto the target material. Subsequent SEM/EDS analysis of the re-sputtered interfaces revealed significant reductions in interface voids formation and enhanced surface uniformity, thereby demonstrating the efficacy of this methodology in refining interfacial quality, which will be discussed in detail in Section V.

Step 3, Nb-target pre-sputtering (Figure 3c). The niobium target is positioned at the cavity aperture and connected to the RF power source, while the copper cavity remains grounded. A 2-minute Ar^+ plasma exposure (0.5 Pa, 150 W RF) removes the native Nb_2O_5 oxide layer via reactive ion etching, yielding an atomically clean sputtering surface.

Step 4, Nb-target sputtering (Figure 3d): The target is translated to the cavity center (maintaining RF-powered Nb and grounded cavity configuration). Nb film growth proceeds under optimized HiPIMRS conditions (current constant: 1 A, duty cycle: 50%, RF frequency: 40 kHz), enabling high ionization (>70% Nb^+ fraction) for uniform coverage of internal surfaces. Film growth kinetics and microstructure evolution are analyzed in Section IV.

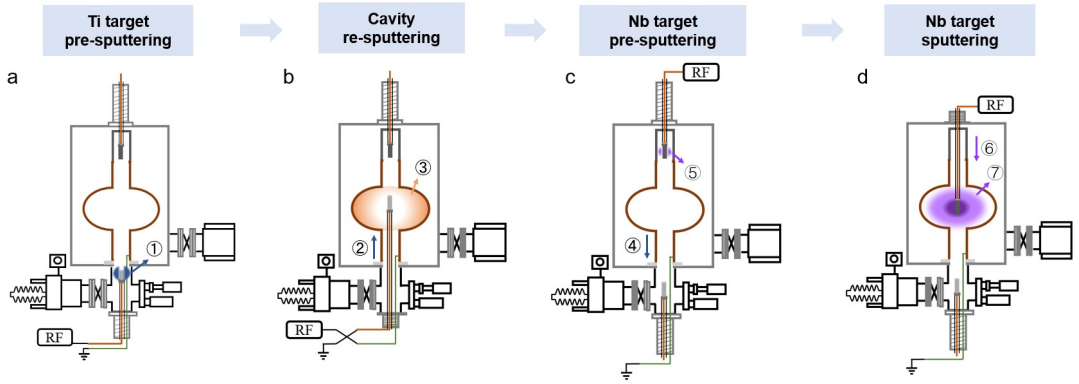

Figure 3. Schematic representation of in-situ re-sputtering substrate treatment and coating procedures. (a) ① illustrates the plasma luminescence emanating from the titanium target. (b) Re-sputtering treatment process achieved by reversing the electric potentials between the niobium target insert and the copper cavity. ② illustrates the elevation of the titanium target to the equatorial plane of the cavity for plasma treatment. ③ depicts the luminous emission manifesting upon the copper cavity surface during this plasma cleansing procedure. This operation primarily serves to eliminate adventitious particulates from the copper cavity while concurrently enhancing its surface asperity. (c) Target preparation via off-site pre-sputtering prior to insertion into the copper cavity. ④ depicts the retraction of the titanium target from the cavity, while ⑤ illustrates the pre-sputtering treatment of the niobium target. This procedure principally serves to eliminate surface contaminants from the niobium target. (d) Sputtering deposition of niobium films. Note the switch of RF power during re-sputtering and sputtering process. The niobium target is positioned at the spherical cavity ⑥ for thin-film deposition via sputtering ⑦. The color representation illustrates the trajectories of different particles: black denotes electrons, blue indicates impurity ions adhering to the copper substrate, and purple represents the flux of argon ions.

III. Nb film growth technique

Prior to niobium deposition, an oxygen-free copper cavity (99.99% purity) was subjected to a multi-stage surface preparation process to attain the nanoscale smoothness and surface cleanliness necessary for film growth. Initially, the copper cavity was polished with silicon carbide papers in a sequence of P500, P1500, and P3000 grit under a continuous coolant flow to minimize work hardening. Then, the cavity surface was refined using a diamond suspension (0.1 μm particle size, Kemet LIQUID DIAMOND) on synthetic polishing cloths, resulting in a mirror finish (R_a < 50 nm). The third step involves immersing the cavity in ultrasonic baths of acetone (10 min, 40 kHz) followed by isopropanol (10 min, 40 kHz) to remove organic residues and polishing media. Finally, the cavity was rinsed in a three-stage cascade of deionized water (18.2 MΩ·cm) with progressively decreasing conductivity and then dried using nitrogen-gas knife to prevent recontamination.

The optimized sputtering technique are carried out as following:

(1) Target location. Position-dependent variations in target substrate distance (Δd = 39-105 mm) within the axis-symmetric cavity necessitates real-time modulation of sputtering parameters to ensure uniform film properties. To address this, our system integrates a high-precision vertical stage (±0.1 mm resolution) that dynamically

synchronizes: pulsed power (0.1-5 kW/cm²) and Ar^+ mass flow (10-100 sccm). This compensation maintains consistent ion flux density across all cavity regions, mitigating Δd-induced plasma non-uniformities.

(2) Substrate heating. Substrate heating during magnetron sputtering critically governs adatom mobility, interfacial diffusion kinetics, and microstructural evolution in Nb films. Maintaining the copper cavity at 500 ± 5°C via radiation heating (tantalum filaments) promotes: (a) enhanced surface diffusion which suppress void/columnar growth; (b) Nb (110) texture development via thermodynamically favored grain growth; (c) interfacial reaction kinetics which can reduced Nb/Cu interdiffusion width to <15 nm; (d) residual stress relaxation. Crucially, this temperature regime remains below copper's recrystallization threshold, preserving substrate integrity.

(3) Ar gas pressure. The argon gas pressure critically governs plasma characteristics, deposition uniformity, and resultant film properties in magnetron sputtering. At low pressures (<0.01 Pa), extended mean free paths reduce gas-phase scattering, yielding dense films due to energetic particle bombardment. However, this regime suffers from impractically low deposition rates (<50 nm/min) and poor thickness uniformity (>15%), rendering it unsuitable for conformal micrometer-scale Nb coatings required in SRF cavities. Conversely, high-pressure operation (>1 Pa) promotes thermalization of sputtered species through frequent collisions, increasing deposition rates but concurrently inducing microstructural defects. These include high porosity (void density $>10^8$ cm^{-2}), gas trapping, and columnar growth – all detrimental to superconducting performance. To balance these competing factors, we optimized the argon pressure to 0.05–0.08 Pa. This intermediate range sustains sufficient ionization for uniform coverage while maintaining adequate adatom mobility to achieve void-free, (110)-oriented Nb films with thicknesses exceeding 3 μm, as verified by cross-sectional SEM (Section IV).

(4) HiPIMRS pulse parameter optimization. Systematic parameter optimization was established under the following impulse sputtering conditions for Nb film growth. Constant-current operation (1.0 A) stabilizes plasma discharge while maintaining voltage within the optimal range of 280–350 V. This voltage window corresponds to ion energies (10–50 eV) that suppress defect formation while ensuring adequate adatom mobility. Position-dependent voltage compensation adjusts for impedance variations across the cavity geometry. We also optimized the impulse source with frequency of 40 kHz and duty cycle of 50%, which can induce a higher deposition rate and enhance the superconducting transition temperature.

Table 1. Detailed process parameters for distinct process steps, primarily encompassing five procedural steps and eight specific parameters.

	Pressure (Pa)	Bias voltage (V)	Current (A)	Power (W)	Time (min)
Pre-sputtering (Ti)	0.5	250-350	0.2	60	2
Re-Sputtering (Ti)	0.5	550-650	0.1	60	5

Pre-sputtering (Nb)	0.5	250- 350	0.5	150	120
Sputtering (Nb, Equator)	5.7	280-320	1.0	300	180
Sputtering (Nb, Tube)	5.7	280-320	0.8	240	180

IV. Structure and superconductivity analysis

Initial parameter optimization was performed using oxygen-free copper substrates mounted within a cylindrical steel test cavity geometrically identical to the standard 1.3 GHz SRF design. Figure 4a-b present comparative optical micrographs confirming conformal niobium film growth across the hemispherical copper surface-spanning from the iris to equatorial regions. This full-coverage result validates the effectiveness of our dynamic positioning system in achieving uniform coating over complex curvatures.

Superconducting properties of the Nb films were characterized via four-point probe resistivity measurements using a Physical Property Measurement System (PPMS, Quantum Design). Figure 4c displays the temperature-dependent resistance of the Nb-Cu sample, where the superconducting transition temperature (T_c) was defined at 90% of the normal-state resistance (R_N). The measured T_c = 8.5 K approaches the bulk Nb value (9.2 K), indicating high film purity and crystallinity. Magneto-transport analysis (Figure 4d) reveals a sharp superconducting-to-normal transition under applied magnetic fields. The upper critical field ($\mu_0 \boldsymbol{H}_c^2$) reaches 2.8 T at 1.8 K, a 40% enhancement over bulk Nb (2.0 T at 1.8 K). These exceptional transport properties demonstrate both high-quality Nb film growth and the efficacy of our HiPIMRS apparatus for conformal superconducting coatings on complex SRF cavity surfaces.

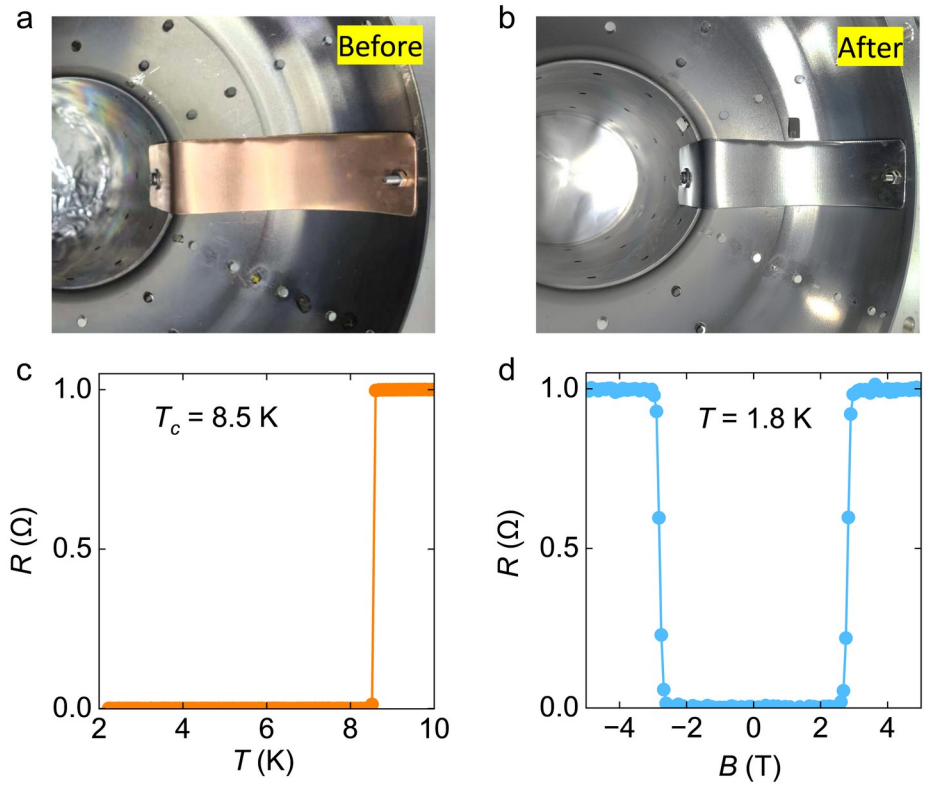

Figure 4. Growth and electrical transport characterization of superconducting films on copper-based substrates. (a) Oxygen-free copper pieces are fixed to the inner surfaces of the stainless-steel cavity. (b) Oxygen-free copper substrates, following a two-hour niobium film deposition, underwent a chromatic metamorphosis from an initial purplish-red to a silvery-white luster. (c) Temperature dependent resistance of superconducting films at zero magnetic field. The superconducting transition temperature is 8.5 K. (d) Magnetic field dependent resistance at 1.8 K. The upper critical magnetic field is 2.8 T, and lower critical magnetic field is 2.6 T. The critical magnetic field of the niobium film exhibited a notable enhancement compared to its bulk counterpart.

To elucidate the intricate microstructural characteristics of superconducting Nb films, a suite of morphological characterizations was meticulously executed. Figure 5a presents the AFM topography (5×5 μm² scan area) of a 3-μm Nb film on Cu substrate, revealing low surface roughness (R_a = 18.5 ± 2.1 nm), uniform grain distribution with average grain size (160 ± 10 nm) and homogeneous nucleation without dendritic growth or voids. Figure 5b displays the XRD pattern, showing a dominant Nb (110) peak at 2θ = 38.5° (d-spacing = 2.34 Å). The strong (110) texturing confirms preferential growth along the superconducting-favorable bcc orientation. Minimal secondary peaks indicate phase-pure Nb without detectable NbO_x phases.

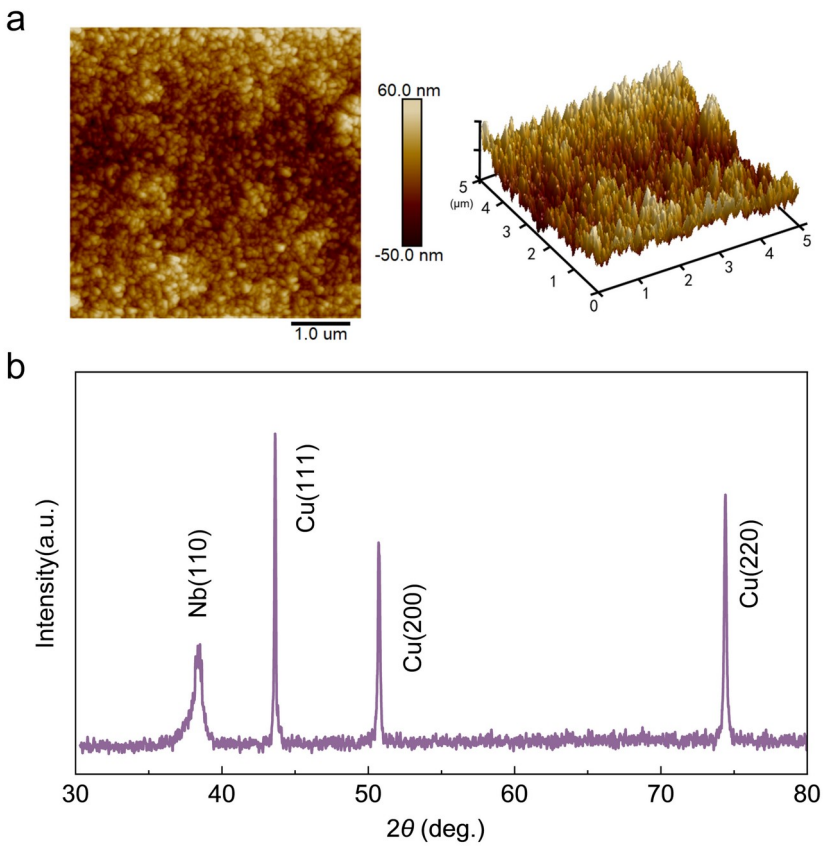

Figure 5. Characterizations of HIPIMRS-deposited Nb films. (a) Atomic force microscopy (AFM) images showing the topographic morphologies in Nb film with nanosized grains. (b) X-ray diffraction pattern showing the phase identification of monophasic Nb film deposited on Cu substrate.

The microstructural evolution of niobium films was quantitatively characterized via scanning electron microscopy (SEM) as a function of impulse current. Figure 6a compares surface morphologies of films deposited at 0.2 A, 0.5 A, 0.75 A, and 1 A, revealing distinct correlations between grain architecture and superconducting performance. The non-superconducting film (0.2 A) represents sub-10 nm nanocrystalline grains, 30-50 nm width network of microcracks and groove-like surface defects (≥1 μm length) indicating incomplete coalescence and high residual stress. In contrast, superconducting Nb films with a low T_c (6.5 K at 0.5 A) exhibited agglomerations of nano-sized grains and limited grain boundary diffusion suggesting inhibited grain growth. Those inhomogeneities were not seen in Nb films with higher T_c values (8.0 and 8.5 K at 0.75 and 1 A), the latter displaying well-faceted polycrystalline grains with an average size of approximately 100 nm and continuous, crack-free morphology. Notably, a strong positive correlation exists between grain size and T_c, where increased impulse current enhances grain growth kinetics, reducing intracrystalline defects that otherwise suppress Cooper pair formation. This microstructure-transport relationship confirms that grain boundary density governs flux-pinning behavior in thin-film Nb superconductors.

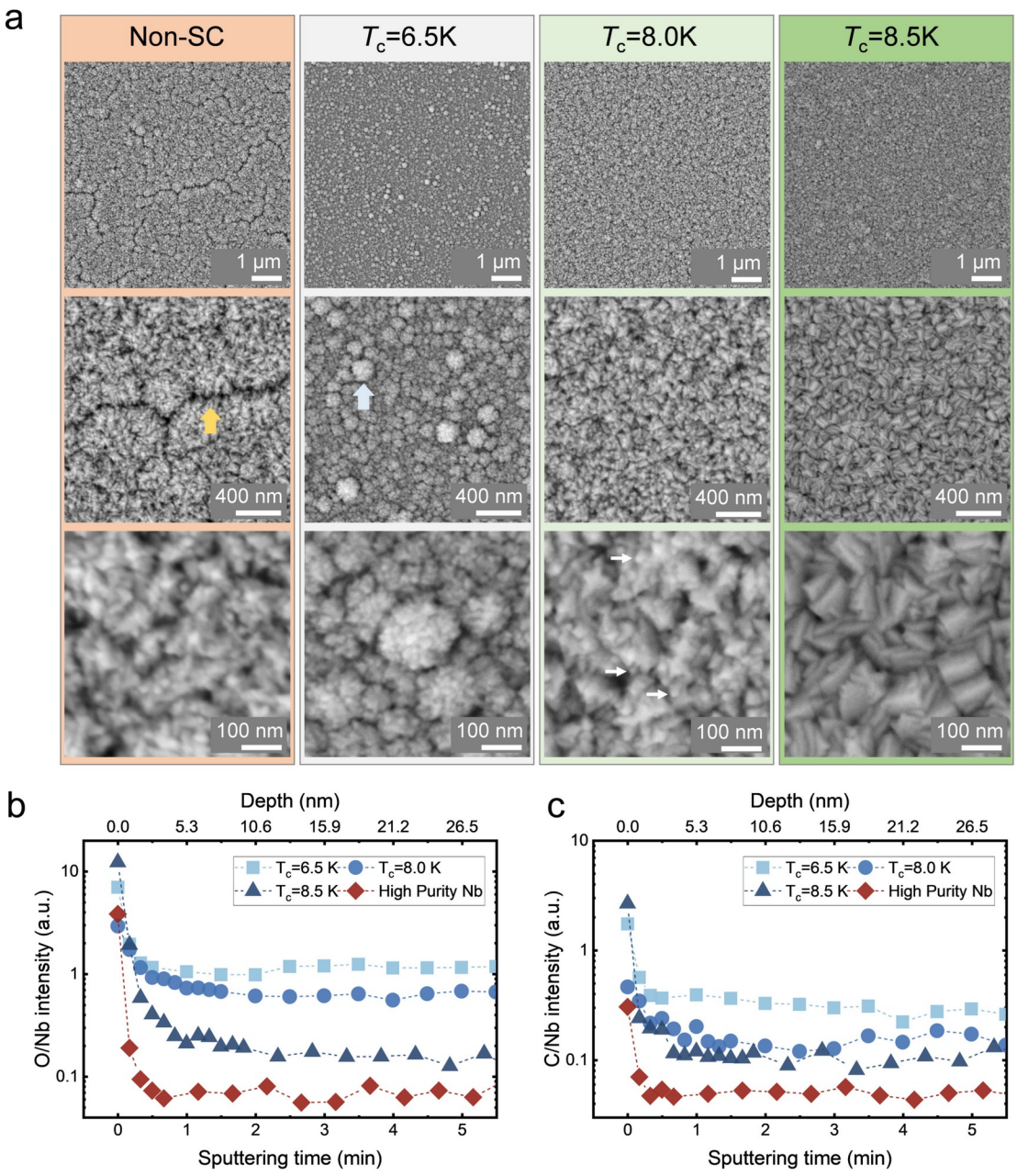

Figure 6. The morphological characteristics of Nb films. (a) Scanning electron micrographs (SEM) showing the surface morphologies of non-superconducting/normal conducting (non-SC) and superconducting films with different transition temperatures (*T*c), which were deposited at different impulse current of 0.2 A, 0.5 A, 0.75 A and 1 A, respectively. The wide arrows mark inhomogeneous morphologies exhibiting grooves (yellow) and spherical agglomerates (blue) on the film surface. The thin arrows mark nano-grains (white). An average grain size of approximately 84 ± 34 nm is estimated from the SEM image (T_c=8.5K). (b) An in-depth profile for O measured by auger electron spectroscopy. (b) An in-depth profile for C measured by auger electron spectroscopy.

The impurity compositions, specifically carbon (C) and oxygen (O), were analyzed using Auger Electron Spectroscopy (AES)[31, 32]. Depth profiling was generated via cyclic Ar^+ sputtering off the surface layers. The results, as shown in

Figure 6b and 6c, indicate that a reduction in the concentrations of O and C beneficial for T_c enhancement. Eventually, the high-T_c film exhibits low concentrations of impurities, as referred by high-purity bulk niobium (RRR≥300). Previous studies have suggested that these impurities tend to segregate at defective sites, such as grain boundaries and dislocations [33]. Combined with the morphological observations, it is inferred that a reduction in grain boundary density and impurity levels is advantageous for T_c enhancement.

The films characterization provides further guidance for process optimization. Particularly, the film quality in terms of grain growth and impurities level can be further improved by applying synergistic substrate heating and variable substrate bias for coatings at different coating positions. Previous studies have shown that crystalline defects, grains connectivity, and grain size may be improved with a higher substrate temperature, which provides higher surface mobility [28]. For copper cavities, the substrates may not allow heating to high enough temperatures due to low melting temperature of copper. The missing energy may then be supplied by ion bombardment (by increasing bias voltage), in which scenario surface and sub-surface processes that are activated the energy of the ions arriving at the surface [34].

V. Interfacial analysis

Building on our earlier discussion of the HiPIMRS process, the in-situ re-sputtering treatment proves critical for enhancing the Nb/Cu interfacial integrity. To quantify this effect, we conducted systematic cross-sectional microstructural analysis comparing HiPIMRS-processed samples with conventionally deposited counterparts. For cross-sectional analysis, samples were prepared using a commercial argon ion polisher (JEOL IB-19520CCP) with sequential ion energies of 8 kV and 6 kV to obtain a smooth surface.

Cross-sectional analysis of conventionally deposited Nb films (without re-sputtering treatment) reveals significant interfacial defects. Figure 7a-b present SEM micrographs of the Nb/Cu interface, where EDS mapping confirms the presence of discrete interfacial voids (10-40 nm width), which can result in stress concentration at void peripheries and oxygen enrichment along void surfaces. This defective interface precipitates adhesion failure, evidenced by spontaneous Nb film delamination after 60 days of ambient storage (Figure 7c). The delamination morphology exhibits classic buckling patterns characteristic of compressive stress release, confirming weak interfacial bonding energy.

In stark contrast to untreated substrates, re-sputtered Cu surfaces enable void-free Nb/Cu interfaces (Figure 7d-e). EDX analysis reveals an interdiffusion zone at the interface rather than a discrete boundary, confirming atomic intermixing that enhances interfacial adhesion. Crucially, no Nb film delamination is observed after thermal cycling (Figure 7f), demonstrating exceptional mechanical stability. Conventional processing invariably produces a native oxide passivation layer (Cu_2O/CuO, 2-5 nm thick) at the Nb/Cu interface (Figure 7a-b), which degrade adhesion strength and suppresses superconducting coherence length. However, the in-situ re-sputtering process eliminates this oxide layer prior to Nb deposition via low-energy

Ar^+ bombardment (50-150 eV) and chemical reduction mechanisms. This yields oxide-free interfaces and reduced interfacial strain which is expected to significantly improve the mechanical stability of the film and thermal conductivity between the film and substrate, thereby reducing the impact of thermal contact resistance [25].

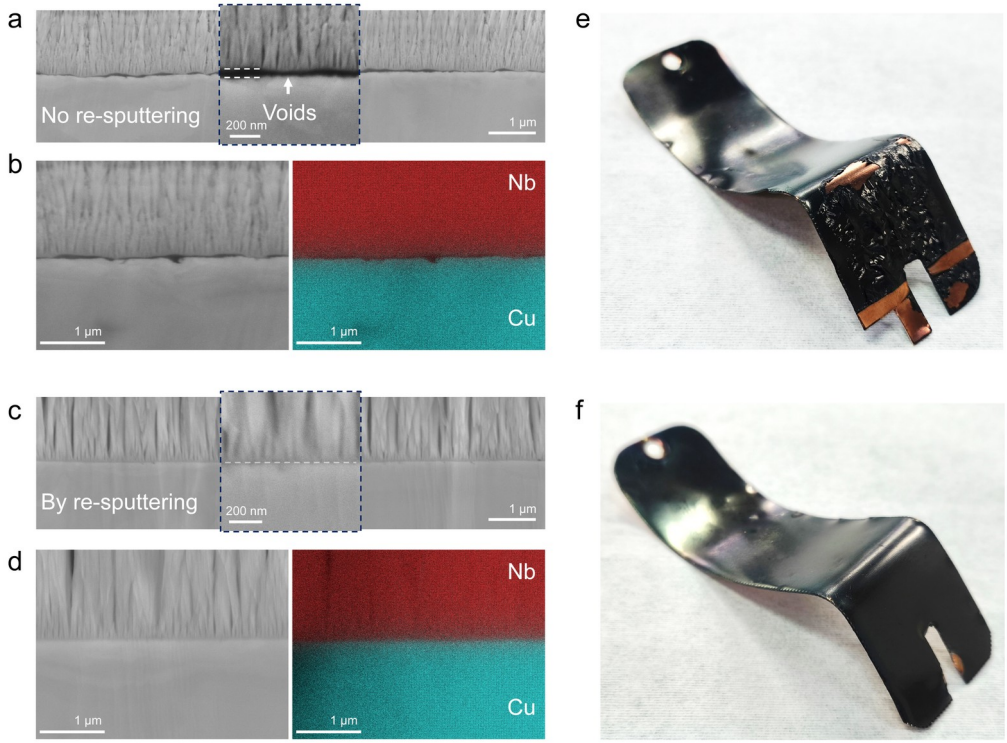

Figure 7. Comparative analysis of the interfacial properties of HiPIMRS-deposited niobium films by no re-sputtering and re-sputtering-treated Cu substrates. SEM and EDS analysis showing the interface morphologies and chemical compositions without re-sputtering(a-b) and re-sputtering(d-e). The inserts in (a)(d) provide magnified view at the interface boundary. (c) Optical inspections showing conformal delaminated films without re-sputtering after 60 days. (f)A photo showing no film delamination by re-sputtering after 120 days.

VI. 1.3 GHz Nb-Cu cavity

Utilizing the optimized HiPIMRS protocol, we deposited niobium films onto the interior surface of a 1.3 GHz copper cavity (Figure 8a). The cavity was subjected to coarse polishing and precision mirror-finishing through commercial-grade machining equipment. The fabrication of 1.3 GHz Nb-Cu cavity is referred by the multi-step sputtering process for the HiPIMRS technique as discussed in Section II-C. During the Nb deposition, the sputtering parameters are as follows: the RF source was in the constant-current mode as a stabilized current of 1 A, frequency of 40 kHz, and duty cycle of 50%; the Ar gas pressure is 6×10^{-2} Pa; the Cu cavity is heated to 500 °C.

Figure 8b presents photographs of the deposited Nb films on the inner walls of the Cu cavity, demonstrating full coverage and uniform film growth across the cavity's interior. To investigate the film adhesion properties, the Nb-Cu cavity was stored in atmosphere (22±2°C, 45±5% RH) for six months. Subsequent observations (Figure 8c) confirmed exceptional adhesion between the Nb films and the copper

substrate, with no detectable delamination attributed to the in-situ plasma substrate treatment methodology.

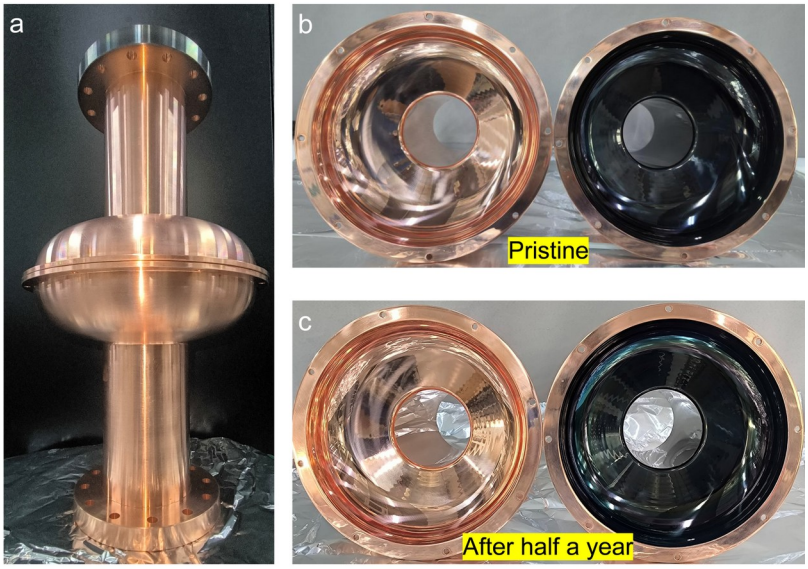

Figure 8. 1.3 GHz copper cavity inner wall coated with deposited superconducting niobium film. (a) 1.3 GHz copper cavity. (b) Upon the initial sputtering deposition of superconducting films on December, 2024, a comparative analysis of the copper cavity revealed entirely coating across inner surfaces. Subsequent observation conducted on June, 2025, confirmed the absence of delamination or structural compromise within the superconducting layers.

VII. CONCLUSIONG AND OUTLOOK

The persistent challenge in copper cavity coating technology is achieving uniform, adherent superconducting films despite extreme target-substrate distance variations (Δd = 39-105 mm) inherent in SRF cavity geometries. While it is known that the presence of a magnetic field can effectively improve the quality of the films, technical challenges remain in instrument design, such as integration of target translation, magnet and water cooling. Although a niobium target with integrated magnet has been designed to enable magnetron sputtering, it only allows that magnetron sputtering has been achieved on selective areas of the target, with deliberately modulated magnetic field distributions across distinct regions, making it difficult to achieve uniform film growth.

In this work, we introduced the design and operational methodology of a novel high-energy pulsed magnetron sputtering apparatus, primarily encompassing magnetron sputtering target system, vacuum acquisition system and in-situ re-sputtering substrate treatment. The target system allows for wide-range movement within a high-vacuum chamber, features adjustable power output in multiple forms, and maintains a consistent relative magnetic field position. This magnetron sputtering target system effectively improves the uniformity and adhesion of the sputtered film. Furthermore, we conducted various tests on the sputtered film’s electrical properties, mechanical properties, and optical properties, which demonstrated the apparatus’ feasibility and enhancement of film performance. This process remains in the

exploratory phase, and further optimization of experimental parameters is necessary to achieve more optimal results.

In summary, we demonstrate that miniaturized target design, integrated magneto-target assembly, and high-power-density operation with uniform magnetic field constraints collectively enable high-quality superconducting Nb films on complex SRF cavity geometries. Our target architecture provides a scalable pathway for copper-cavity coating technology, optimizing the process and design in conformal deposition and thermal management, which will enable next-generation superconducting accelerators.

ACKNOWLEDGMENTS

This research was supported in part by the Ministry of Science and Technology (MOST) of China (No. 2022YFA1603903), the National Natural Science Foundation of China (Grants No. 12004251, 12104302, 12104303), the Science and Technology Commission of Shanghai Municipality (Grant No.21YF1429200, 23YF1426900, 21JC1405100), Natural Science Foundation of Shanghai (Grants Nos. 25ZR1402374, 25ZR1402368, and 25ZR1401252), and China's double first-class project funds of ShanghaiTech University. We also thank SoftNano Laboratory, Center for High Resolution Electron Microscopy (CħEM), and Analytical Instrumentation Center (AIC) of School of Physical Science and Technology, ShanghaiTech University.

AUTHOR DECLARATIONS

Conflict of Interest

The authors have no conflicts to disclose.

Author Contributions

Peng Dong: Data curation (equal); Investigation (lead); Methodology (equal); Software (equal); Writing – original draft (equal); Writing – review & editing (equal). **Yanjiang Wang:** Data curation (equal); Investigation (Lead); Methodology (equal); Software (equal). **Jianjun Xiao:** Data curation (equal); Investigation (Lead); Methodology (equal); Software (equal). **Meiling Bao:** Methodology (equal). **Xin Liu:** Methodology (Supporting). **Zhaoxi Chen:** Data curation (equal); Methodology (equal); Writing – original draft (equal); Writing – review & editing (equal). **Jinfang Chen:** Methodology (Supporting). **Dong Wang:** Methodology (Supporting). **Xuerong Liu:** Methodology (Supporting). **Yulin Chen:** Methodology (Supporting). **Zhi Liu:** Methodology (Supporting). **Jun Li:** Conceptualization (lead); Project administration (lead); Visualization (equal); Writing – original draft (equal); Writing – review & editing (equal).

DATA AVAILABILITY

The data that support the findings of this study are available from the corresponding authors upon reasonable request.

References:

1. Padamsee, H., *50 years of success for SRF accelerators—a review.* Superconductor Science and Technology, 2017. **30**,053003.
2. Padamsee, H., *<RF Superconductivity>*. Science, Technology, and Applications, 2009.
3. Ciovati, G., et al., *Development of a prototype superconducting radio-frequency cavity for conduction-cooled accelerators.* Physical Review Accelerators and Beams, 2023. **26**(4).
4. Padamsee, H., *Superconducting Radiofrequency Technology for Accelerators*. 2023, Wiley-VCH.
5. K. C. Dominic Chan Los Alamos National Laboratory, L.A., *<Application_of_RF_superconductivity_to_a_high-current_linac.>*. IEEE TRANSACTIONS ON APPLIED SUPERCONDUCTIVIm, 1999. **9**(2).
6. Valente-Feliciano, A.-M., *Superconducting RF materials other than bulk niobium: a review.* Superconductor Science and Technology, 2016. **29**(11).
7. Arzeo, M., et al., *Enhanced radio-frequency performance of niobium films on copper substrates deposited by high power impulse magnetron sputtering.* Superconductor Science and Technology, 2022. **35**(5).
8. Posen, S. and D.L. Hall, *Nb3Sn superconducting radiofrequency cavities: fabrication, results, properties, and prospects.* Superconductor Science and Technology, 2017. **30**(3).
9. Leith, S., et al., *Superconducting NbN thin films for use in superconducting radio frequency cavities.* Superconductor Science and Technology, 2021. **34**(2).
10. G. Terenziani, S.C., T. Junginger, I.A. Santillana, CERN, Geneva, Switzerland, *Nb Coating Developments With HiPIMS For SRF Application.* 2013.
11. Calatroni, S., *20 Years of experience with the Nb/Cu technology for superconducting cavities and perspectives for future developments,*. Phys. C Supercond. its Appl., 2006. **441**: p. 95–101.
12. C. Benvenuti, S.C., I. E. Campisi,a P. Darriulat, M. A. Peck, R. Russo and A.-M. Valente, *<Study_of_the_surface_resistance_of_niobium_sputter-coated_copper_cavities.pdf>*. IEEE TRANSACT1ONS ON APPLIED SUPERCONDUCTIVITY, 1999. **9**(2).
13. C.Benvenuti, S.C., P.Darriulat, M.A. Peck, A.-M. Valente# and C.A. Van 't Hof,, *<Study of the Residual Resistance of Superconducting Niobium Films at 1.5 GHz.pdf>*. Phys. C Supercond. its Appl., 2001. **351**(4): p. 421–428.

14. M. Burton, A.P., L. Phillips, A.M. Valente-Feliciano†, and C. E. Reece, *RF Results of Nb Coated SRF Accelerator Ccvities Via HiPIMS.* LINAC2018, 2018.

15. A. Bendavid*, P.J.M., T.J. Kinder, E.W. Preston, *The deposition of NbN and NbC thin films by filtered vacuum cathodic arc deposition.* Surface and Coatings Technology 2003. **163-164**: p. 347–352.

16. Kanetoshi Shibataa, H.I., Noboru Yugamib, Tadaomi Miyazakic, Yasushi Nishidab, *Production of Nb thin film by ECR sheet plasma.* Thin Solid Films, 2001. **368**(2): p. 291–294.

17. M. Burton, A.P., A.M. Valente-Feliciano†, and C. E. Reece, *Progress with Nb HiPIMS Films on 1.3 GHz Cu Cavities.* 19th Int. Conf. on RF Superconductivity, 2019.

18. Tuckmanel, J., <*The LEP2 superconducting RF system*>. IEEE Transactions on applied superconductivity, 1999. **9**(2): p. 270–275.

19. Miyazaki, A. and W. Delsolaro, *Two different origins of the Q -slope problem in superconducting niobium film cavities for a heavy ion accelerator at CERN.* Physical Review Accelerators and Beams, 2019. **22**.

20. Ramiere, A., C.Z. Antoine, and J. Amrit, *Model for hot spots and Q-slope behavior in granular niobium thin film superconducting rf cavities.* Physical Review Accelerators and Beams, 2022. **25**(2): p. 022001.

21. Willson, S.A.H., Aiden V. Shpani, Liana Do, Van Lew-Kiedrowska, Helena Liepe, Matthias U. Transtrum, Mark K. Sibener, S. J., *Impact of submicron Nb_3Sn stoichiometric surface defects on high-field superconducting radiofrequency cavity performance.* Physical Review Research, 2024. **6**(4).

22. R Ries, E.S., F Gömöry, A Medvids, C Pira and O B Malyshev, *Superconducting properties and surface roughness of thin Nb samples fabricated for SRF applications.* Journal of Physics: Conference Series, 2019. **1559**(012040).

23. Ghaemi, M., et al., *Growth of Nb films on Cu for superconducting radio frequency cavities by direct current and high power impulse magnetron sputtering: A molecular dynamics and experimental study.* Surface and Coatings Technology, 2024. **476**.

24. Lee, J., et al., *Grain-boundary structure and segregation in Nb3Sn coatings on Nb for high-performance superconducting radiofrequency cavity applications.* Acta Materialia, 2020. **188**: p. 155–165.

25. Palmieri, V. and R. Vaglio, *Thermal contact resistance at the Nb/Cu interface as a limiting factor for sputtered thin film RF superconducting cavities.* Superconductor Science and Technology, 2016. **29**(1): p. 015004.

26. E. Chyhyrynets†, O.A., R. Caforio1, D. Fonnesu, D. Ford, G. Keppel, C. Pira, A. Salmaso, F. Stivanello, G. Marconato1, *Plasma Electrolytic polishing technology progress development for Nb and Cu substrate preparation.* 21th Int. Conf. RF Supercond., 2023.

27. Turner, D.A., et al., *Investigating the Superconducting Properties and Surface Morphology of Sputtered Nb Films on Cu Due to Laser*

Treatment. IEEE Transactions on Applied Superconductivity, 2023. **33**(4): p. 1–12.

28. Leith, S., et al., *HiPIMS deposition of superconducting Nb thin films onto Cu substrates.* Vacuum, 2023. **212**: p. 112041.

29. Benvenuti, C., et al., *Study of the surface resistance of superconducting niobium films at 1.5 GHz.* Physica C: Superconductivity, 1999. **316**(3): p. 153–188.

30. Benvenuti, C., et al., *Fluxon pinning in niobium films.* Physica C: Superconductivity, 2001. **351**(4): p. 429–437.

31. Chen, Z.-X., et al., *Compositional study of δ-NbN film by Auger electron microscopy.* Tungsten, 2022.

32. Chen, Z., et al., *Unraveling the Nanoscale Segregation Mechanism in N-Doped Niobium for Enhanced SRF Performance.* Small Methods, 2024. **n/a**(n/a): p. 2301319.

33. Wang, C.-Y., et al., *Microscopic examination of rf-cavity-quality niobium films through local nonlinear microwave response.* Physical Review Applied, 2024. **22**(5): p. 054010.

34. Colligon, J.S., *Energetic condensation: Processes, properties, and products.* Journal of Vacuum Science & Technology A, 1995. **13**(3): p. 1649–1657.